frontiers | Frontiers in Soft Matter

TYPE Original Research
PUBLISHED 18 July 2023
DOI 10.3389/frsfm.2023.1221803

OPEN ACCESS

EDITED BY
Kay Saalwächter,
Martin-Luther-University Halle-Wittenberg, Germany

REVIEWED BY
Damien Montarnal,
Laboratoire de chimie polymérisation procédés et matériaux, France
Mostafa Ahmadi,
Johannes Gutenberg University Mainz, Germany

*CORRESPONDENCE
Jasper Feng,
j.feng@fz-juelich.de
Wim Pyckhout-Hintzen,
w.pyckhout@fz-juelich.de

RECEIVED 12 May 2023
ACCEPTED 28 June 2023
PUBLISHED 18 July 2023

CITATION
Feng J, Allgaier J, Kruteva M, Förster S and Pyckhout-Hintzen W (2023), Constraining effects on polymer chain relaxation in crosslinked supramolecular dual networks.
Front. Soft. Matter 3:1221803.
doi: 10.3389/frsfm.2023.1221803

Constraining effects on polymer chain relaxation in crosslinked supramolecular dual networks

Jasper Feng[1,2]*, Jürgen Allgaier[1], Margarita Kruteva[1], Stephan Förster[1,2] and Wim Pyckhout-Hintzen[1]*

[1]Neutron Scattering and Biological Matter (JCNS-1/IBI-8), Forschungszentrum Jülich GmbH, Jülich, Germany, [2]Institute of Physical Chemistry, RWTH Aachen University, Aachen, Germany

Polymer networks containing transient physical and permanent chemical cross-links exhibit unique mechanical properties due to the intrinsic reassociating ability of supramolecular functional groups. Similar to supramolecular gels, these networks allow the controlled release of stored energy and can extend the life of polymer networks in practical applications. In this study, we investigated the rheology, dielectric spectroscopy, stress–strain behavior, and dynamic mechanical analysis of networks based on long polybutylene oxide (PBO) chains functionalized with randomly placed thymine (Thy) side groups. A transient network was formed by proportionally mixing this matrix with short non-entangled linear 1,3,5-diaminotriazine (DAT) head–tail modified PBO chains, exploiting the hetero-complementarity of the DAT–Thy triple hydrogen bond. This transient polymer network was further cross-linked to a dual network via a thiol-ene click reaction to form static covalent bonds. In PBO, the similar polarity of the PBO matrix and the DAT–Thy functional groups ensures that the molecular chain motion is not affected by segregation, resulting in a homogeneous polymer phase without microphase-separated functional group domains. Dielectric relaxation spectroscopy was combined with rheology to quantify the relaxation processes of the interconnected polymers and the strength of the DAT–Thy bonding interactions in the melt. The results showed two distinct plateaux in the relaxation modulus due to contributions from hydrogen and permanent bonds. In the case of the dual network, the lifetime of the hydrogen bond was prolonged and higher activation energy was observed due to the physical cross-link preventing the movement of the long chain.

KEYWORDS

rheology, dielectric spectroscopy, dual network, DMA, supramolecular polymer, Thy-DAT, hydrogen bonding

1 Introduction

Rubber materials are widely utilized in numerous applications, ranging from seals and joints between different materials to tires and vibration dampers (Friedrich and Almajid, 2013; Jiang et al, 2014). Their applications play an exceedingly significant role in the area of aerospace engineering (Vahdati and Saunders, 2002), automobile engineering (Chandra and Kumar, 2017; Barrera and Tardiff, 2022), and material science (Hamed, 2000; Suslick et al, 2023). However, the limitations of conventional rubbers, such as susceptibility to fatigue, impact, abrasion, and wear, are the major causes of premature failure (Saintier et al, 2011; Awaja et al, 2016), leading to frequent replacements and substantial investments.

As a consequence, the limited service life of conventional rubbers necessitates frequent replacements, resulting in significant costs and operational downtime. Incorporating weak-bond concepts similar to those found in living matter, which prevent localized stress peaks when under high mechanical load, would be tremendously advantageous (Gold et al, 2016; Shoda et al, 2020) to extend service time and optimize ultimate properties. Achieving this goal requires an interdisciplinary approach that combines microscopic and macroscopic studies aimed at understanding fundamental principles. Non-covalent interactions, including host–guest (Lee et al, 2011; Pappalardo et al, 2012; Kawano et al, 2022), hydrogen bonds (Lange et al, 1999; van Gemert et al, 2011; Verjans et al, 2022), and metal–ligand interactions (Le Bohec et al, 2016; Mozhdehi et al, 2016; Bentz and Cohen, 2018), are now recognized to exhibit both time and inherent temperature dependencies, which are coupled with specific chemistry. The range of interactions covers a binding energy spectrum from around 1–100 kJ/mol and includes diverse types, among which hydrogen bonding interactions, as they occur in natural base-pair combinations, offer a remarkable advantage for self-healing (Murphy and Wudl, 2010; Xie et al, 2021), as well as for the development of adaptive and/or responsive materials, without the need for introducing potentially hazardous heavy ions or metals. Pre-emptive damage control, however, is a much more important mechanism than self-healing for extended use problems and a topic of recent investigations.

We had discovered in the past that the bioinspired combination of thymine (Thy) and diaminotriazine (DAT) as active H-bonding entities—as synthetic analogs to thymine–guanine nucleobase conjugation (Li et al, 2011)—in a polymer matrix of polybutylene oxide (PBO) exhibited ideal time scales for the lifetime of the closed state (Allgaier et al, 2016). An illustrative application of this from daily life is tires. Although these are already highly vulcanized and reinforced, the process of opening and re-closing bonds enables the tire to respond in a self-sufficient manner to actual road conditions. The supramolecular bonds behave as so-called sacrificial bonds and allow the modulus of the rubber to vary between soft and strong in timescales of 0.001–0.01 s in a typical temperature range between −25 and +25 degree Celsius. Taking into account typical micro- and macro-textural asperities (e.g., 0.001, 1 mm) and speeds of the order of 100 km/h, impact frequencies of the order of 100–1,000 Hz are encountered that thus fit ideally to the frequencies at which supramolecular H-bonds dissipate their stored energy and switch between higher and lower modulus. In this frequency range, the rolling resistance is optimized, fuel consumption is reduced, and premature abrasion and wear due to local overstresses is minimized. In addition, transient PBO-comb polymers, combined with monofunctional DAT-arms associating with randomly located Thy-counterparts on long chains and even transient networks of the same when bifunctional DAT-arms were used, have already been reported (Staropoli et al, 2016; Staropoli et al, 2020). However, it is important to consider the compatibility of the overall mixture, as unfavorable interactions between monomer and functional end group chemistries can lead to the formation of micelles, which often limits controlled applications. Nonetheless, if compatibility is achieved, it allows for a rather unique determination of the characteristic response times.

Although covalent networks formed through vulcanization or random linking with peroxides or radiation—with or without fillers—have good mechanical properties, especially in terms of reversibility of deformation, the addition of reversible, physical, and transient crosslinks to such permanent networks leads to the creation of (auto-) responsive dual networks. These networks exhibit novel dependencies on strain or temperature that can be essential for advanced processing methods or applications, where the transient links allow for external control (Shangguan et al, 2017; Katashima, 2021). The ability of hydrogen bonds to associate and dissociate, as demonstrated in our work, becomes a valuable tool for triggering the overall mechanical behavior of such dual networks, ranging from highly elastic to very soft. These dual networks consist of both chemical and physical crosslinks and are similar to swollen networks or hydrogels (Vereroudakis et al, 2020; Nicolella et al, 2021).

However, the practical use of gels has been limited by their relatively low elastic moduli. To overcome this limitation, the incorporation of high-density hydrogen bonding into a polymer melt can significantly enhance the significance of transient bonding. This, in turn, enables the development of new self-repairing and self-damage-avoiding materials as explained previously for tires, as well as the processing of special branched polymers where transient bonds provide an intrinsic plasticizing property.

In this study, we, therefore, aim to synthesize and characterize dual networks that take advantage of both the PBO backbone polymer and supramolecular hydrogen bonding moieties, specifically Thy and DAT, and to permanently crosslink long chains through a thiol-ene reaction. To the best of our knowledge, this work is the first in the open literature which is based on homogeneity, hetero-complementary supramolecular activity, and covalent random crosslinking in the melt state. Unlike gel systems, our transient crosslink is mobile and consists of a short polymer chain that interconnects different long polymer chains, minimizing self-looping, and thus affects the behavior of the matrix chain in a more defined and rather controlled way. We use rheology and dynamic mechanical analysis to compare the behavior of a transient network (TN) prior to, and a dual network (DN) after, bulk-crosslinking the former transient network while preserving all chain interactions like entangling and H-bonding. Dielectric relaxation spectroscopy is attracted with a special focus on the bifunctional linker. Our results show that the encaging of transient linkages within the mesh of the permanent network affects the lifetime of the H-bond positively. Finally, we successfully compare the equilibrium properties of the DN to those obtained in a non-linear stretching experiment and pave the way for future studies in this area. Our findings highlight the potential for the development of new materials with enhanced mechanical properties by exploiting transient bonding mechanisms. This research has significant implications for the design of advanced materials with unique and tunable properties.

2 Experiment methods

2.1 Synthesis

Supplementary Schemes S1, S2 in the Supplementary file show the reaction synthesis scheme for the long- and short-chain polymers, respectively, while the previous literature (Allgaier et al, 2016) and Supplementary Section 1.3 in the Supplementary

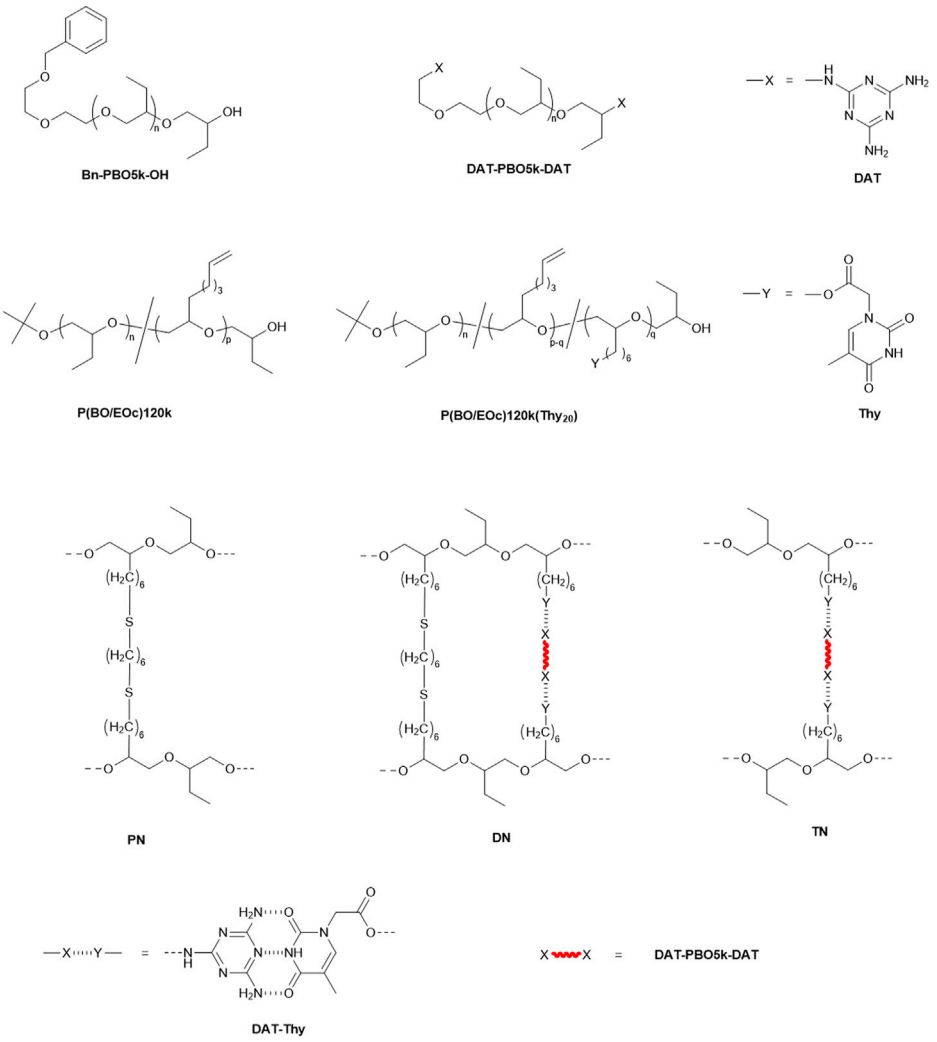

FIGURE 1
Structures of PBO precursors, functionalized samples, and network structures. Unfunctionalized short-chain (Bn-PBO5k-OH) and long-chain (P(BO/EOc)120k) components and functionalized short-chain (DAT-PBO5k-DAT) and long-chain (P(BO/EOc)120k(Thy_{20})) were investigated as reference polymers.

file provide further details on their synthesis. The structure of the polymer precursors and networks are indicated in Figure 1. The average number of vinyl groups per P(BO/EOc)120k(Thy_{20}) chain is 28.2. The functionalization of the end-standing double bonds of the comonomer to thymine leads to an estimated number of thymine units of 19.7 in P(BO/EOc)120k(Thy_{20}) as determined by the integral of the corresponding peaks in the NMR spectrum of the long chain. The remaining unreacted vinyl groups are used for further thiol-ene crosslinking reactions. The crosslinking method for the network is presented in the Supplementary file, Section 2.

2.2 Characterization

2.2.1 Rheology

Oscillatory rheology has been used to probe the flow properties of the polymer melt. The measurements were performed on both ARES (Rheometric Sci) and ARES G2 (TA Instruments) systems in dynamic mode using standard 8-mm parallel plates. Frequency–temperature sweep tests were conducted in the frequency region with $\omega = 0.1...100$ rad/s and a temperature ramp between −55°C and 25°C in steps of 5° for TN samples and 10° for all other polymer melt samples. The temperature was controlled by a liquid nitrogen blanket. The soaking time to achieve thermal equilibrium was 300 s for each temperature. The strain amplitude was 1% with the sample loading thickness of roughly 1 mm. Master curves with a reference temperature $T_0 = -25$°C were generated by the TRIOS software, and a 2D shifting algorithm was applied.

2.2.2 Broadband dielectric spectroscopy

Dielectric properties were measured using a dielectric spectrometer (Novocontrol Technologies) equipped with an alpha impedance analyzer (Novocontrol Technologies) covering a frequency range from 10^{-7} to 10^{-2} Hz. The temperature was controlled by a Quattro system (Novocontrol Technologies)

TABLE 1 Swelling degree and calculated mesh size. The correlation between soluble material and the fraction of short chains is virtually 100%. In the PN network, the measured sol fraction is mostly related to an unused HDT crosslinker and no chain scission was detected.

	DN	DNref	PN
Q	10.02	12.17	5.54
Φ_{sol} (%)	22.45	25.28	2.34
M_c (g/mol)	18,700	25,300	6,260

TABLE 2 Glass transition temperature and molecular weight for different polymers.

	T_g (°C)	M_n (kg/mol) (SEC)	PDI (SEC)
TN	−65.1	-	—
Bn-PBO5k-OH	−67.5	5	1.02
DAT-PBO5k-DAT	−63.6	5	1.02
P(BO/EOc)120k	−67.3	120	1.12
P(BO/EOc)120k(Thy_{20})	−64.1	120	1.08

from −55°C to 25°C, with temperature steps of 10°C for each sample. Melt samples and two 0.5-mm diameter glass fiber spacers were placed between the 20-mm diameter Au-coated electrodes. Network samples were directly placed in between the electrodes.

2.2.3 Size-exclusion chromatography

To determine the molecular weight of polymers, size-exclusion chromatography (SEC) was conducted on an Agilent 1260 Infinity SEC instrument with Wyatt DAWN Heleos II light scattering (LS) detector and an Optilab T-rex differential refractive index detector. The experiment was carried out using three PolyPore columns at 50°C and a solvent mixture consisting of tetrahydrofuran (THF), N,N-dimethylacetamide (DMA), and acetic acid (84:15:1 by volume) at a flow rate of 1 mL/min. The differential refractive index of polymer samples was calculated by the ASTRA software with the value of 0.0049.

2.2.4 Differential scanning calorimetry

Differential scanning calorimetry (DSC) analysis was carried out using a Q2000 DSC analyzer (TA Instruments). A temperature range from −120°C to 20°C with a heating/cooling rate of 10°C/min was analyzed.

2.2.5 Dynamical mechanical analysis

Dynamic mechanical analysis (DMA) was carried out on a Q800 DMA analyzer (TA Instruments) in tension mode. Networks were cut into a rectangular shape with dimensions of 25 mm × 4 mm × 1 mm. The storage modulus and loss modulus were obtained in dynamic oscillatory tests. Data were collected as a function of temperature in the range −55 to +25°C, covering a frequency range from 0.1 to 100 Hz with a 5 min soaking time and 1% strain amplitude. All the measurements were performed under a nitrogen atmosphere.

2.2.6 Mechanical characterization

Tensile tests were conducted on an ARES (Rheometric Sci) system, cooled with liquid nitrogen, exploiting the normal force measured by the 2KFRTN1 transducer and using home-made clamps. The samples were cut to a shape of 10 mm × 1 mm × 1 mm. Tensile deformation was performed within a range of strain rates varying from 0.106 s^{-1} to 0.0067 s^{-1} with careful temperature control. The deformed samples were reused to perform the same strain rate-dependent experiments.

The degree of cross-linking of a polymer network can be characterized from equilibrium swelling experiments using the Flory–Rehner equation, which is expressed in gravimetric terms as follows:

$$\phi_{sol} = \frac{m_{network} - m_{dried}}{m_{network}}, \tag{1}$$

$$Q = \left(\frac{m_{swollen}}{m_{dried}} - 1\right)\frac{\rho_{PBO}}{\rho_{tolu}} + 1, \tag{2}$$

$$\frac{\rho_{PBO}}{(1-\phi_{sol})M_{c,swell}} = \frac{\rho_{PBO}}{(1-\phi_{sol})M_w} + \frac{-\left[\ln\left(1-Q^{-1}\right) + Q^{-1} + \chi Q^{-2}\right]}{V_{mol,tolu}\left(Q^{-\frac{1}{3}} - \frac{1}{2}Q^{-1}\right)}, \tag{3}$$

where $m_{swollen}$ refers to the mass of the network after being swollen by the solvent, toluene, and m_{dried} is the mass of the network after it has been redried in a vacuum for 4 days. The density of PBO is 0.95 g/cm^3. The density of toluene is 0.86 g/cm^3. ϕ_{sol} refers to the soluble fraction in the network. χ is the Flory–Huggins interaction parameter between toluene and PBO. The value was calculated to be 0.35 since the cohesion parameter between the two components was negligible and the contribution arose only from entropy (Van Krevelen and Te Nijenhuis, 2009). V_{tolu} is the molar volume of toluene (106 mol/cm^3). $M_{c,swell}$ represents the experimental mesh size of the network. The degree of swelling of the network is tabulated in Table 1. The short-chain polymers (DAT-PBO5k-DAT and Bn-PBO5k-OH) without permanent linkage diffuse out of the network upon swelling and constitute the entire sol fraction (ϕ_{sol}). The effective mesh size factor is corrected for the soluble fraction. A permanently linked network (PN) in the same conditions was prepared as well without the short-chain component to sustain the efficiency of the thiol-ene reaction. For samples DN and DNref, in which the active difunctional DAT linker was replaced by the inactive Bn-PBO5k-OH but keeping the Thy-modified long-chain component, this volume fraction correlates well with the volume fraction of the short-chain component.

3 Results and discussion

From the perspective of molecular design, mixtures of P(BO/EOc)120k(Thy_{20}) and DAT-PBO5k-DAT form hydrogen bonds through a variety of complementary interactions, including homo-complementary interactions between thymine and thymine groups (Thy–Thy) and between diaminotriazine and diaminotriazine groups (DAT–DAT), as well as hetero-complementary interactions between thymine and diaminotriazine groups (Thy–DAT) (Herbst et al, 2010; Cortese et al, 2011; Cortese et al, 2012; Brás et al, 2013; Krutyeva et al, 2015). The transient network (TN) obtained from these active components already showed higher viscosity and longer relaxation times at room

10.3389/frsfm.2023.1221803

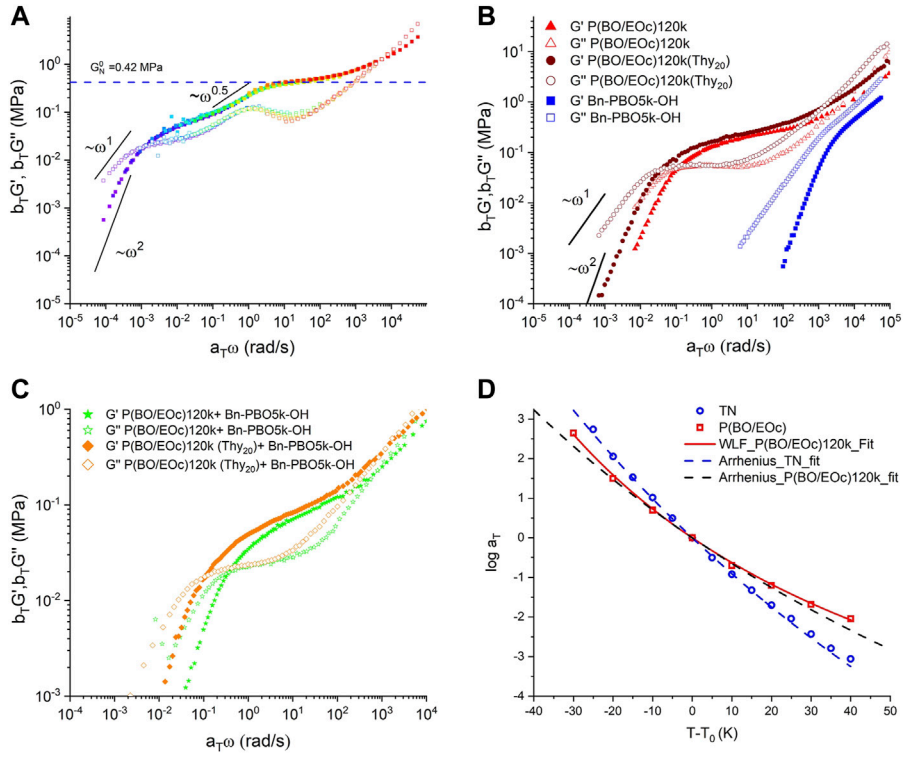

FIGURE 2
(A) Best rheology master curve of storage (solid squares) and loss modulus (hollow squares) of the TN sample at T = 248 K. **(B)** Storage and loss modulus master curve of unfunctionalized (P(BO/EOc)120 k, Bn-PBO5k-OH, functionalized precursor polymers (P(BO/EOc)120 k(Thy$_{20}$)), and **(C)** master curve of their binary mixture.**(D)** Shear modulus time–temperature superposition shift factor of the TN (blue circle) and P(BO/EOc) 120k (red square). The reference temperature T_0 = 248 K. The dashed line (blue for TN and black for P(BO/EOc)120 k) is the fit curve from the Arrhenius fitting (Eq. 8). The WLF fit (Eq. 7, red curve) is applied to the P(BO/EOc)120 k sample.

temperature than the non-functionalized polymer melt. The photo-induced thiol-ene reaction, carried out in the polymer melt state at room temperature, generated a stable dual network (DN) with both transient and permanent bonds and quenches the different topologies. Although the system contains multiple components and relaxation mechanisms, preliminary SAXS (Supplementary Figures S17, S18) at low temperatures confirm a typical RPA or block-copolymer peak, which is the consequence of a correlation gap between correlated blocks. The Thy–DAT complex is treated as a single block and two such blocks are separated by the flexible 5 k PBO chain. The correlation with further blocks in the chain or network is negligible due to the separation distance to the neighboring Thy–DAT unit. It is shown that the scattering vector at high-Q wing follows a Q^{-2} dependence, which is typical of a random walk of the polymer chain, in clear contrast to an expected ~ Q^{-4} decay for microphase-separated Thy–DAT domains. Therefore, the rheological properties of TN are first investigated to gain a better understanding of the behavior of DN.

3.1 Rheology master curve of TN

The material under investigation, TN, is a blend based on P(BO/EOc)120k(Thy$_{20}$) and DAT-PBO5k-DAT with a stoichiometry of [Thy]/[DAT] = 1. The tentative rheology master curve is shown in Figure 2A at the reference temperature T = −25 ° C and shows some deviations due to complex thermorheological behavior related to the H-bonds. Although the time–temperature superposition (TTS) should not apply in view of the different activation energies, the agreement is still rather good. To facilitate comparison, Figures 2B, C depict the corresponding master curves at the same reference temperature for both the unfunctionalized polymer and a mixture containing the same stoichiometry of long- and short-chain components as TN.

The effective storage modulus of TN shows two plateaux, the first occurring in the region around ω ~ 1,000 rad/s and having a higher plateau modulus than that of pure P(BO/EOc) and P(BO/EOc)120k(Thy$_{20}$). A second plateau occurs at much lower frequencies after the supramolecular bonds have broken up (*vide infra*). The entanglement modulus G_N^0 of P(BO/EOc) had been estimated in previous work to be 0.30 MPa (Staropoli et al, 2016) at the same temperature of 248 K, although it cannot be excluded that it may depend on the fraction of the EOc comonomer. G_N^0 was estimated in our case from the minimum of tan δ, which corresponds to the modulus where the loss part is minimal. In the master curve, the plateau modulus is therewith higher and extracted as $G_N^0 \approx$ 0.42 MPa. This increase in modulus is attributed to the formation of transient bonds. To estimate the increase in modulus caused by the formation of transient bonds, the mesh size between active transient bonds, denoted as M_t, can be

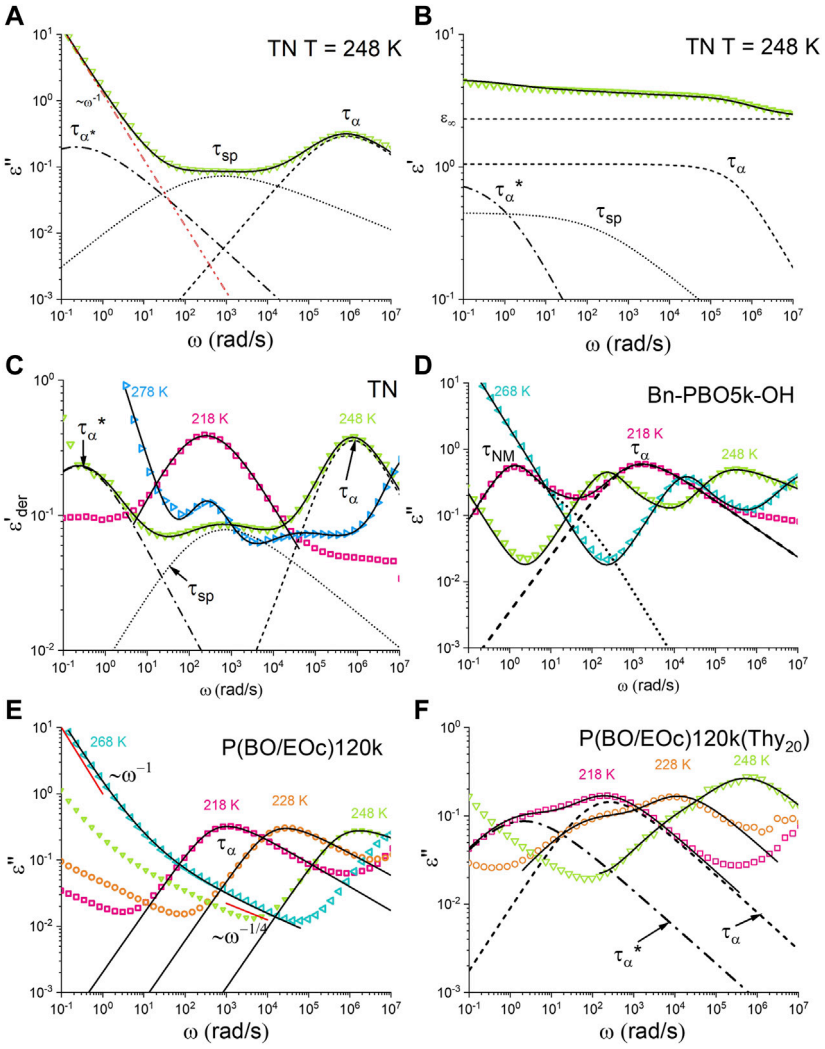

FIGURE 3
Dielectric **(A)** loss, **(B)** storage, and **(C)** derivative of the storage spectrum of the TN sample at T = 248 K. Dashed lines present α relaxation at different temperatures from (Eqs 10, 11). Dotted curves show the normal mode relaxation of side products, one-side-supramolecularly attached oligomers, and dotted dash curves correspond to the α* relaxation process. Solid curves are the summation of all the relaxation curves. Dielectric loss spectra of **(D)** Bn-PBO5k-OH, **(E)** P(BO/EOc)120 k, and **(F)** P(BO/EOc)120 k(Thy_{20}) are shown. The solid line represents the fit from the summation of the Havriliak–Negami equation. The dashed lines present the fits of **(D)** α relaxation and normal mode relaxation **(F)** α relaxation and α* relaxation.

calculated by the summation of both transient bonds and entanglement contributions:

$$G_N^0 = \rho RT\left[\frac{1}{M_e} + \frac{1}{M_t}\right] = G_e + G_t. \quad (4)$$

The equation involves several variables, where R represents the gas constant, ρ corresponds to the polymer density, and M_e denotes the entanglement molecular weight of PBO, which is equivalent to ~8,000 g/mol. G_e is the entanglement modulus, and G_t is the modulus contribution of transient bonds. The calculated results indicate that M_t is ~11,200 g/mol, i.e., 10.7 transient bonds out of 19. Seven bonds attach the linker chain to the backbone at T = 248 K. The effective G_e value is lower than that reported in the literature on pure PBO (Gerstl et al, 2010) and 0.3 MPa by Staropoli et al. (2016) because our estimates by formula 4 did not take into account that the short component dilutes and expands the width of the entanglement tube (Doi and Edwards, 1978) when the transient bonds are far out in the non-association stage. Binary blends of two polymers, one of them having entanglement molecular weight smaller than that of the other, show reduced moduli due to tube diameter expansion, commonly referred to as the dynamic dilution effect (van Ruymbeke et al, 2014; Shahid et al, 2017). To explore more complex scenarios in TN, we compared the mixture of long and short molecular weight in-active PBO to understand the modulus decrease caused by dynamic dilution, shown in Figures 2B, C. For a binary blend of P(BO/EOc)120k and Bn-PBO5k-OH, the short unentangled Bn-PBO5k-OH acts like a theta solvent and increased the tube diameter of the long P(BO/EOc)120k. The rheology curve showed a reduction in the entanglement modulus and an acceleration of the reptation process in the dilated tube. The modulus was expressed as a function of the volume fraction, $G_N^0(\phi) = G_N^0\phi^{(1+\alpha)}$, where α is fixed to 1 due to the theta

TABLE 3 Vogel–Fulcher–Tammann fit parameters of the segmental relaxation.

Sample	B	T_0 (°C)	T at τ_α = 100 s (°C)	τ_0 (s)
Bn-PBO5k-OH	895	−106	−72	4.16e-10
P(BO/EOc)120k	644	−94	−70	3.38e-10
P(BO/EOc) 120k(Thy_{20})	364	−81	−65	1.47e-8
DN	658	−91	−67	6.92e-11
TN	918	−101	−65	3.59e-11

conditions. ϕ is the volume fraction of the long component. For the stoichiometry of the initial mixture $\phi_0 = 0.71$, this gives a modulus decrease of 50%. The same modulus decrease was also observed when comparing pure P(BO/EOc)120k(Thy_{20}) with a mixture of P(BO/EOc)120k(Thy_{20}) and Bn-PBO5k-OH.

Considering the TN case, the association number of supramolecular pairs affects the dilution effect of the entanglement modulus G_e. The relationship between the plateau modulus and the dynamic dilution effect in the TN is expressed as follows:

$$G_N^0(\phi) = \rho RT\left[\frac{\phi^{1+\alpha}}{M_e} + \frac{1}{M_t}\right] = G_e(\phi) + G_t. \quad (5)$$

The volume fraction is determined by the stoichiometry of the initial mixture ϕ_0 and the fraction of the connected supramolecular pairs N_x/N_c, where N_x is the number of actual connected stickers and N_c is the number of total stickers. In this case, N_c stands for the total number of thymine units along P(BO/EOc)120k(Thy_{20}) ($N_c = 20$). The volume fraction increased by the number of associations can be derived as $\phi = \phi_0 + (1 - \phi_0)N_x/N_c$. Here, $N_x - 1 = M_w/M_t$ and M_w is the molecular weight of the long component, which is 120 kg/mol. The plateau modulus as a function of N_x could be rewritten as follows:

$$G_N^0(N_x) = \rho RT\left\{\frac{\left[\phi_0 + (1-\phi_0)\left(\frac{N_x}{N_c}\right)\right]^{1+\alpha}}{M_e} + \frac{(N_x - 1)}{M_w}\right\}, \quad (6)$$

where N_x determines both the transient mesh size and the diluted entanglement mesh size. At T = 248 K, the TN sample displayed a G_e of 0.21 MPa and G_t of 0.21 MPa corresponding to M_t = 9,110 g/mol and N_x = 14.2. Here, the equipartition is purely fortuitous. These results suggest that about approximately 70% of the hydrogen bonds were active and contributed to network formation. Previous research conducted by Staropoli et al., 2016 on a very comparable system with a comb structure reported an association ratio of ~80% at the same temperature (T = 248 K). The somewhat lower crosslink density observed in our TN case, compared to the corresponding supramolecularly branched polymers, could be attributed to a more limited accessibility of Thy for a free DAT sticker when this is already restricted on one side by a terminal anchor linkage. A similar effect is observed for short-chain branching in polyolefins (McLeish, 2002) for which the effect of an un-entangled arm is smeared out.

To discuss the deceleration of the TN terminal time, the sticky reptation model (Leibler et al, 1991) could be used to describe the complex system. To begin with the simplest system, P(BO/EOc) 120k(Thy_{20}), the Thy–Thy association pairs can also form a TN. The whole curve would shift horizontally to lower frequencies, i.e., longer times. The plateau modulus is apparently not increased by the Thy–Thy association, indicating that the Thy–Thy bonds must have already dissociated in the intermediate-frequency range. Considering the PBO structure with a lower number of thymine groups (Allgaier et al, 2016), a smaller shift factor was observed consequently. In both cases, the Thy–Thy lifetime is shorter than the Rouse relaxation time of a strand between the sticky points. (Chen et al, 2016). The shift toward longer times could be the result of increased 'smeared' friction and a change in T_g. The measurement of T_g from DSC is shown in Table 2. The differences in T_g lead to different shifts in their respective master curve reference temperatures. Since the data are not iso-frictional, at the high-frequency range, the modulus of sample P(BO/EOc)120k(Thy_{20}) is higher than that of sample P(BO/EOc)120k. The association and dissociation behavior of Thy–Thy bonds will be further discussed in the dielectric spectrum analysis.

In accordance with the sticky reptation model on the TN sample (Figure 2A), the storage modulus displays a power law of $G' \sim \omega^{0.5}$ in the intermediate regime (Wu and Chen, 2022), where the different modes of the sticky reptation process are gradually relaxing. The system behaves as Rouse-like relaxation, indicating that once the transient bonds detach, the subchains relax. At even lower frequencies, hydrogen bonds no longer exert significant influence, and instead, the network which was primarily determined by entanglements, gives rise to a lower modulus due to the increased mesh size. In the terminal zone, the chains undergo flow with $G' \sim \omega^2$ and $G'' \sim \omega^1$. DAT–DAT associations, neither cyclic nor polycondensation, do not occur again due to the high dilution. Cluster-trapped relaxation is not observed in the case of our homogeneous polymer blends (Goldansaz et al, 2016).

In Figure 2A, the TTS master curve is not strictly applicable in the region ω ~ 1,000 rad/s, as observed by deviations in the loss modulus. The reason for the deviation is the varying number of hydrogen bonds at different temperatures. The region of deviation could be a good starting point to investigate the relationship between temperature and the number of association groups. The results could yield the relative activation energy of the transient bonds in the network. The experimental shift factor a_T is shown in Figure 2D. For ordinary polymers like P(BO/EOc) 120k, devoid of any functional groups, the empirical Williams–Landel–Ferry (WLF) relation fits well. By using the WLF equation, it is possible to account for the impact of temperature.

$$\log\ a_T = \frac{-c_1^0\left(T - T_{ref}\right)}{c_2^0 + \left(T - T_{ref}\right)}. \quad (7)$$

In addition to the WLF equation, an Arrhenius correlation can also be used to determine the activation energy for a particular temperature range:

$$\log\ a_T = \frac{2.303E_a}{R}\left[\frac{1}{T} - \frac{1}{T_{ref}}\right]. \quad (8)$$

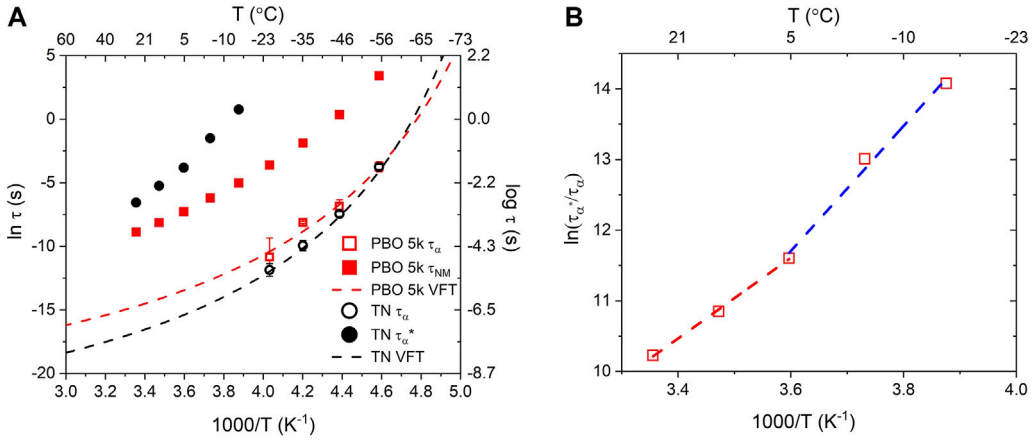

FIGURE 4
(A) Dielectric peak relaxation time of the Bn-PBO5k-OH α relaxation (hollow red square), normal mode relaxation (solid red square), TN α relaxation (hollow black circle), and α* relaxation (solid black circle). Both α relaxation modes are fitted to Vogel–Fulcher–Tammann (VFT) (Eq. 14), with fitting parameters summarized in Table 3. **(B)** Arrhenius plot of the TN sample from Eq. 15.

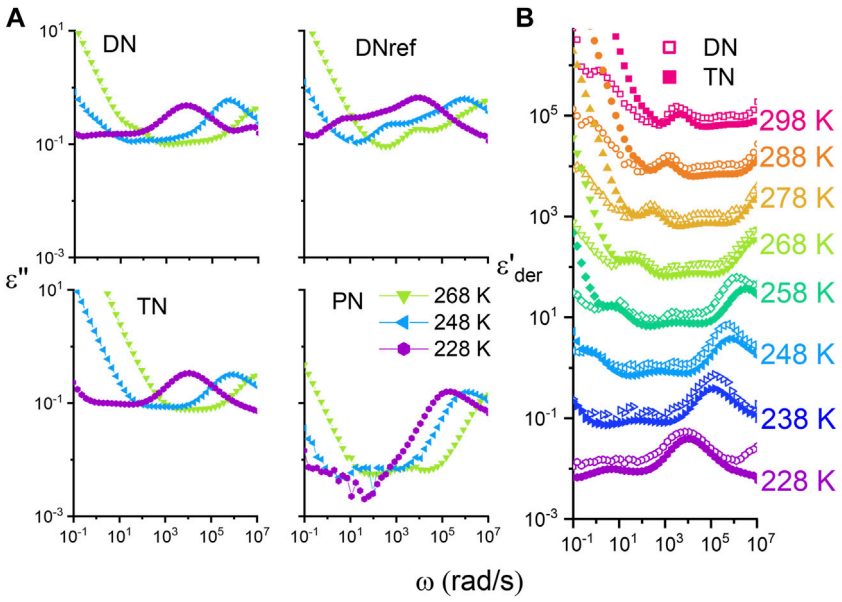

FIGURE 5
(A) Dielectric loss permittivity of network samples at different temperatures. **(B)** Derivative of storage modulus of the DN and TN. The curves for the different temperatures are shifted by 1 decade upwards for clarity reasons.

Here, the gas constant is denoted by R and the reference temperature is represented by T_{ref}, which is equal to −25°C. The activation energy is denoted as E_a.

Assuming that a single activation process takes place in the interval of hydrogen bonding from the temperature region ΔT = 10 K with reference temperature T = 248 K, the Arrhenius fitting gives the activation energy of the TN as 111 kJ/mol. If the same Arrhenius fitting is applied to the same temperature range for P(BO/EOc)120 k, its activation energy is 79 kJ/mol. The difference is 32 kJ/mol, corresponding to the activation energy of the triple hydrogen bonds, i.e., about 10 kJ/mol per H bond. The extracted total activation energy is smaller but of similar magnitude as the quadruple hydrogen 2-ureido-4 [1*H*]-pyrimidinone (UPy) bonds (Ahmadi et al, 2022). The activation energy of the polymer chain dynamics is thus offset by the difference of the two energies. To separate the contribution of other dynamic processes responsible for the increase of the total activation energy, broadband dielectric spectroscopy (BDS) is applied.

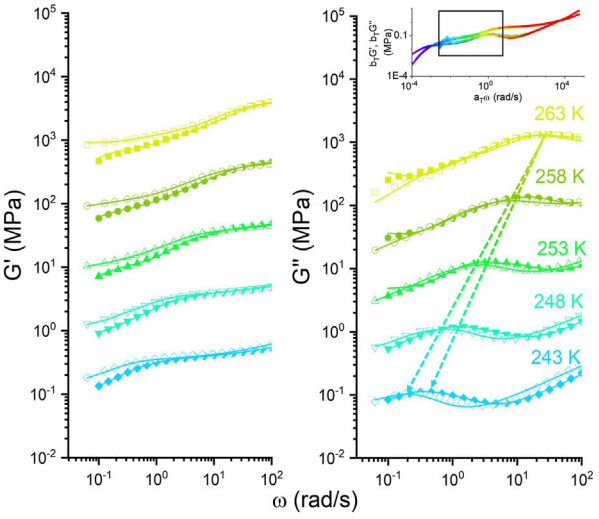

FIGURE 6
Storage modulus of the TN (hollow) and DN (solid) samples derived from dynamic mechanical analysis and small amplitude oscillatory shear rheology. The relation $E^* = 3G^*$ was applied. The curves are shifted by 1 decade vertically for each temperature for clarity reason. The unshifted curve refers to T = −30°C. The inset on the top right marks the investigated range in the master curve of TN. The frequency range focuses entirely on the opening mechanism of the H-bond.

3.2 Dielectric spectroscopy for dipole relaxation

Dielectric analysis could provide further microscopic insight into the molecular mechanism. The dipole moments of the PBO monomers are aligned parallel to the chain backbone and summed up, which classifies PBO as a type A polymer according to the Stockmayer classification (Stockmayer, 1967). The sum of these dipole moments gives an end-to-end net polarization vector, and the loss rate curve (ε'') shows two relaxation processes. Dielectric measurements are thus useful to investigate the timing of hydrogen bond breakage, as the dipole moment changes when the transient groups dissociate, leading to a change in the permittivity and gaining an additional peak in the loss permittivity spectrum. Therefore, dielectric measurements are a valuable method for studying the lifetime of transient hydrogen-bonded groups. The typical loss permittivity spectrum obtained from dielectric spectroscopy exhibits signatures of two distinct relaxation processes, i.e., of fast motions corresponding to the PBO segmental relaxation (α relaxation) observed at high frequencies and slow dielectric relaxation response attributed to the global chain motion (Watanabe, 2001; Yamane et al, 2005; Glomann et al, 2011; Urakawa et al, 2018). In order to quantify the dielectric response from our samples, we obtain the relaxation time by fitting the spectra with an empirical Havriliak–Negami (HN) function shown as follows (Havriliak and Negami, 1967):

$$\varepsilon^*_{HN}(\omega) = \varepsilon_\infty + \frac{\Delta\varepsilon_{HN}}{[1 + (i\omega\tau_{HN})^\alpha]^\beta}, \tag{9}$$

τ_{HN} represents the characteristic relaxation time of the detected process and $\Delta\varepsilon_{HN}$ corresponds to the number of relaxing dipoles in the external field. In addition, $\varepsilon_\infty = \lim_{\omega\tau \gg 1} \varepsilon'(\omega)$, which leads to

$$\varepsilon''_{HN}(\omega) = \Delta\varepsilon_{HN}\left[1 + 2(\omega\tau_{HN})^\alpha \cos\left(\frac{\pi\alpha}{2}\right) + (\omega\tau_{HN})^{2\alpha}\right]^{-\beta/2} \sin(\beta\phi), \tag{10}$$

$$\phi = \arctan\left[\frac{(\omega\tau)^\alpha \sin\left(\frac{\pi\alpha}{2}\right)}{1 + (\omega\tau)^\alpha \cos\left(\frac{\pi\alpha}{2}\right)}\right]. \tag{11}$$

The peak position is obtained from τ_{HN} as follows:

$$\tau_{max} = \tau_{HN}\left[\frac{\sin\left(\frac{\pi\alpha\beta}{2+2\beta}\right)}{\sin\left(\frac{\pi\alpha}{2+2\beta}\right)}\right]^{1/\beta}. \tag{12}$$

In our case, the instrumental dielectric frequency is reported in rad/s. In some of the samples, the low-frequency relaxation response is smeared out due to the contribution of DC conductivity. Hence, the derivative of storage permittivity response which is not affected by conductivity (See Figure 3B) is used to identify the corresponding peak position as follows (Wübbenhorst and van Turnhout, 2002):

$$\varepsilon'_{der} = -\frac{\pi}{2}\frac{\partial\varepsilon'(\omega)}{\partial \ln\omega}. \tag{13}$$

This approach improved the resolution of peaks in the spectrum, allowing for the detection of relaxation processes with low intensities or those occurring at low frequencies. The fitting function used in this method is based on the literature (Wübbenhorst and van Turnhout, 2002). In summary, the dielectric response of the samples can be described as a combination of a power-law fit for the low-frequency DC conductivity and two HN functions for the high-frequency α relaxation, as well as for the intermediate-frequency global relaxation. For α and β, typical values of 0.5 for α and 0.7 for β were obtained.

The dielectric spectrum of the TN sample is presented in Figure 3A. P(BO/EOc)120k and P(BO/EOc)120k(Thy_{20}) are presented in Figures 3E, F.

Figures 3D–F also show the dielectric loss spectrum, i.e., $\varepsilon''(\omega)$ obtained from the single Bn-PBO5k-OH, P(BO/EOc)120k, and P(BO/EOc)120k(Thy_{20}), respectively. As depicted in Figure 3D, two distinct relaxation processes are observed in Bn-PBO5k-OH. The relaxation time for α relaxation is denoted as τ_α and the global relaxation time, also known as normal mode relaxation, is denoted as τ_{NM}. Notably, τ_α exhibits a non-Arrhenius temperature dependence and hence is approximated using the empirical Vogel–Fulcher–Tammann (VFT) equation shown as follows (Vogel, 1921):

$$\tau_\alpha = \tau_0 \exp\left(\frac{B}{T - T_0}\right), \tag{14}$$

where B and T_0 are the VFT parameters. τ_0 is the segmental relaxation time at temperatures approaching infinity. The temperature for which τ_α = 100 s is taken as the dielectric analog of the glass transition temperature T_g in DSC measurements. The fitting parameters are summarized in Table 3. The dielectric spectrum of the long-chain component shown in Figure 3E also provides valuable insight into the relaxation mode distribution of P(BO/EOc)120k samples. Previous studies (Riedel et al, 2010;

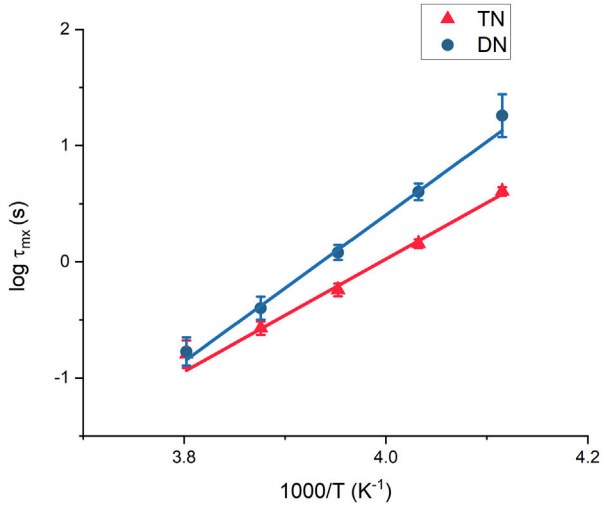

FIGURE 7
Extracted relaxation time (τ_{mx}) by the multi-Maxwell model from the DN (blue circle) and TN (red triangle) samples and the corresponding energy extracted from Eq. 18 of TN = 92.6 kJ/mol and DN = 120.7 kJ/mol.

Glomann et al, 2011) have attributed the power-law decay of $\varepsilon'' \sim \omega^{-1/4}$ in the loss permittivity to the contour length fluctuation process (CLF) in PBO. At lower frequencies, the contribution of DC conductivity masks the normal mode response, as evident from the slope of −1 in Figure 3E.

Comparing the dielectric relaxation of P(BO/EOc)120k (Figure 3E) with that of P(BO/EOc)120k(Thy_{20}) (Figure 3F) reveals the presence of an additional relaxation peak present at frequencies about 2 orders of magnitude lower than those of the alpha relaxation process. This additional peak, termed as α*, is attributed to the binding of the Thy–Thy dimer functional groups. In a closed state, the dipole moment of the complex is 0 but non-zero upon opening.

On the other hand, when the short-chain DAT-PBO5k-DAT is added to form the TN, the α* signal of the Thy–Thy bond disappears as shown in Figure 3A. This is a clear indication that there are at least less competitive Thy–Thy dimer pairs and the formation of DAT–Thy bonds is the thermodynamically stable product. Further comparison of the TN and P(BO/EOc)120k(Thy_{20}) shown in Figures 3A, F (at −25°C) shows that the normal mode relaxation in the TN is shifted to a lower frequency, as chain motion is inhibited in the case of TN (Schaefer et al, 2020).

The TN sample in Figure 3A or the derivative of the real part of the permittivity in Figure 3C, e.g., at T = 248 K, revealed three peaks. In Figure 3C, but best visible at higher temperatures, a peak appears, which correlates with the normal mode relaxation of the DAT-PBO5k-DAT polymer. As the temperature increases, the dissociation of the supramolecular groups induces a normal mode relaxation of the PBO5k chain. This Thy–DAT α* relaxation thus marks the released 5k normal mode motion in the TN in the frequency range 100–1,000 rad/s at T = 278 K. In between the high-frequency α relaxation and the low-frequency α* relaxation, another shallow peak evolves. This relaxation process must be assigned to the polymer side products present in the sample mixture. The relaxation time associated with these side products is denoted as τ_{sp}. The side products may have developed during the synthesis process such as the homocoupling reaction of the DAT-PBO5k-DAT, or due to the conversion limit of the DAT-PBO5k-DAT end group as reported previously (Allgaier et al, 2016). Another possible source of polymer side product relaxation mode could be the contribution of single-ended DAT-PBO5k-DAT, where only one end is attached to the long backbone. The Rouse relaxation time of a single connected side chain is four times longer than that of the free chain. The observation shows that the mean relaxation time of τ_{sp} is somewhat longer than the normal mode relaxation time of Bn-PBO5k-OH.

Figure 4A represents the relaxation time from different temperatures. The relaxation process α* of the TN shows different slope dependence compared to the normal mode relaxation of Bn-PBO5k-OH. To determine the activation energy of the TN, it is necessary to consider the motion of the connected segments and to correct the attempt time for bond dissociation by the segment relaxation time. The following equation is used to estimate the activation energy (Zhang et al, 2017; Ge et al, 2020; Ahmadi et al, 2023):

$$\tau_{\alpha^*}(T) = \tau_{\alpha}(T)\exp\left(\frac{E_a}{RT}\right). \quad (15)$$

The fitted slope in Figure 4B allows the estimation of the association activation energy for TN. The activation energy shows two slopes in the high- and low-temperature regions, corresponding to activation energies of 47.3 and 73.5 kJ/mol, respectively. This indicates that the hydrogen bonds in the TN remain active up to +5°C, whereas at higher temperatures, all bonds are open and the equilibrium state for the supramolecular group would be dissociated. The difference between the energies is 26.2 kJ/mol, which corresponds to the energy scale for triple hydrogen bonds. The higher activation energy at low temperatures suggests that chain dynamics is also involved in the transient binding system (Monkenbusch et al, 2016), and additional energy is required to separate the functional group to a sufficient distance.

The same analysis could now be ideally performed on the DN sample. Crosslinking involves the formation of chemical bonds between polymer chains and effectively freezes in or quenches the orientation of the dipole moments. Likewise, it limits the mobility of charge carriers and results in a reduction in the overall conductivity due to the permanent crosslinks. These facts considerably complicate the analysis of such networks and less sensitivity is expected. Nevertheless, Figure 5 summarizes the difference between the TN and DN with the derivative of the storage permittivity.

Using the derivative of the storage permittivity, at least the DC conductivity can be adequately corrected for.

In this way, only dipolar relaxation processes (α or normal mode) and two different types of polarizations can be observed, i.e., the Maxwell–Wagner–Sillars (MWS) polarization related to interfaces and the electrode polarization (EP) due to blocking of charge carriers at the interface between the ion-conducting material and the electron-conducting metallic electrode. For these polarization mechanisms, the slope at low frequencies is ~ −1.5…−2.0 and therefore considerably higher than −1 and remains visible (Gałązka and Osiecka-Drewniak, 2022).

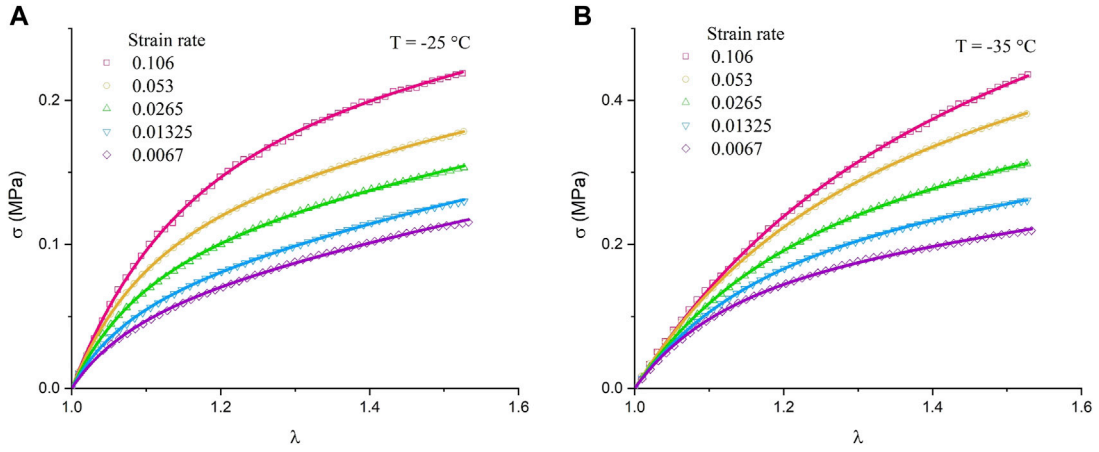

FIGURE 8
Stress–strain curve of the DN sample at different strain rates **(A)** T = −25°C and **(B)** T = −35° C. Solid lines represent fitted curves according to Eq. 19.

At the chosen rheological reference temperature of 248 K, the DN sample broadens and smears toward lower frequencies in comparison to the TN. This is physical and becomes more pronounced at even lower temperatures. This indicates a different slowing down or another temperature dependence compared to the higher T. For T = 258 K and above, the shape of the function of the TN and DN peaks is very congruent and reveals no discrepancies, except for the stronger parasitic polarization effects in the TN. Apparently, the reason for the broadening has vanished, and therefore it could be concluded that the broadening toward longer characteristic times is correlated to the presence of permanent crosslinks.

A full comparison of the investigated networks and mixtures is also summarized in Figure 5 (A). For TN, DN, DNref, and PN, the α transition at the selected temperatures occurs around the same frequency within the accuracy of the measurements. For PN, only the segmental relaxation remains due to the fixed relative positions of the chain end-to-end vectors after crosslinking, as expected. TN and DN data, on the other hand, are not affected by the crosslinked state since the normal mode of the long chain, either crosslinked or not, is out of the experimental window and only the mobile PBO5k chain, as the "label" which does not participate into the permanent network, remains visible. The DNref sample itself clearly shows the relaxation of the short-link chain around 500 rad/s and the weak α* of the Thy–Thy complex around 10^4 rad/s at 248 K. A close inspection of G^* (ω) of these samples shows a comparable weak signature of these as well. We conclude that the comparison between DN and TN is, however, severely hampered by the DC conductivity and polarization effects and cannot reach better-founded conclusions.

3.3 DMA analysis on DN and TN

Figure 6 presents a comparison between the DMA and rheology curves of the DN and TN at varying temperatures. In order to match the dynamic Young's modulus $E(\omega)$ and shear modulus $G(\omega)$ on the same scale, the relationship between Young's modulus and shear modulus is 3, i.e., $E^* = 2(1+\nu)G^* = 3G^*$ for the Poisson's ratio $\nu = 0.5$ of the network. The assumed Poisson number seemingly leads to a perfect agreement in the absolute modulus values. At $T = -30^{\circ}C$, a shift by roughly 1/3 of a decade in the transient bond lifetime of the DN toward longer times is observed.

This may be attributed to the static crosslink hindering the Rouse motion of the elastic chains between them for the DN compared to the TN. At lower temperatures, these permanent static bonds form a cage-like prison or confinement, which impedes the relative motion of the long backbone and extends the lifetime of transient bonds. As a result of the permanent bonds suppressing the basic polymer relaxation, the probability of Thy–DAT sticker pairs opening and attaching to new stickers decreases on small length scales. This is equivalent to the increase in the activation energy barrier for bond cleavage and favors the reassociation ability due to the short PBO chains living in a tube-like cage. To investigate the increase of activation energy between the DN and TN, a phenomenological multi-Maxwell model is used to fit the relaxation processes at different temperatures. For the TN, a contribution of two types of Maxwell models can be considered at low (reptation) and high frequency (hydrogen bonds).

$$G'(\omega) = G_0\omega^{n_g} + \sum_{i=1}^{3} g_{t,i}\frac{\omega^2\tau_{t,i}^2}{1+\omega^2\tau_{t,i}^2} + \sum_{i=1}^{3} g_{p,i}\frac{\omega^2\tau_{p,i}^2}{1+\omega^2\tau_{p,i}^2}, \quad (16)$$

$$G''(\omega) = G_0\omega^{n_g} + \sum_{i=1}^{3} g_{t,i}\frac{\omega\tau_{t,i}}{1+\omega^2\tau_{t,i}^2} + \sum_{i=1}^{3} g_{p,i}\frac{\omega\tau_{p,i}}{1+\omega^2\tau_{p,i}^2}. \quad (17)$$

The characteristic time for the sticker is fitted at each temperature separately without the interference of a possible slightly erroneous TTS shifting. The parameter G_0 is the power law prefactor at short times, and n_g is the slope dependence factor in the dynamic glass transition region, which is 0.5 for Rouse relaxation. g_t and g_p are

10.3389/frsfm.2023.1221803

TABLE 4 Dobrynin–Konkolewicz fitting parameters for Figures 8A, B.

T (°C)	Strain rate (1/s)	G_t (MPa)	G_p (MPa)	G_{tot} (MPa)	τ_{DK} (s)
−25	0.106	0.35	0.097	0.45	3.66
	0.053	0.33	0.097	0.43	4.55
	0.027	0.27	0.091	0.36	8.11
	0.013	0.22	0.089	0.30	11.51
	0.0067	0.18	0.080	0.26	24.56
−35	0.106	0.44	0.090	0.53	17.03
	0.053	0.44	0.089	0.53	22.31
	0.027	0.40	0.085	0.46	32.29
	0.013	0.37	0.080	0.45	49.20
	0.0067	0.35	0.080	0.43	68.52

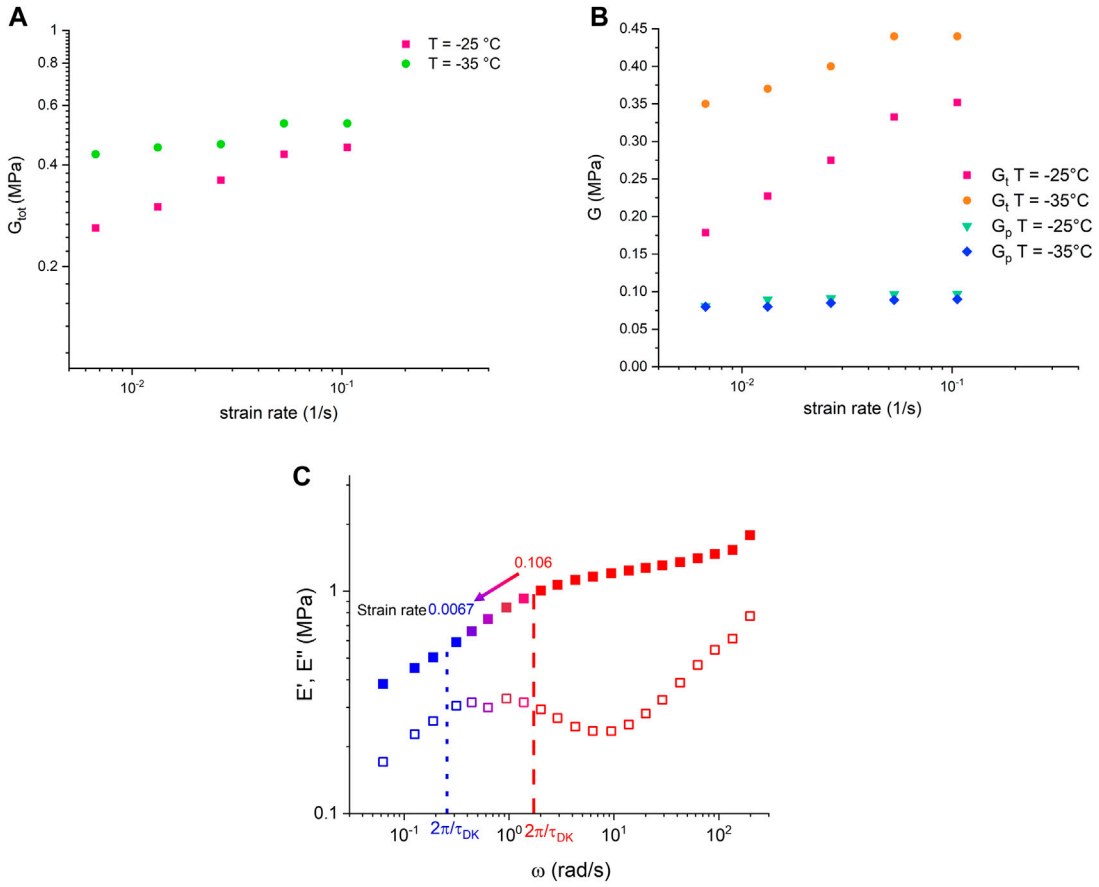

FIGURE 9
(A) G_t and G_p and **(B)** total modulus G_{tot} *vs.* strain rate obtained from the Dobrynin–Konkolewicz model at T = −25 °C and T = −35 ° C **(C)** DMA curve of the DN at T = −25 °C with storage (solid) and loss (hollow) modulus. The characteristic relaxation times obtained by the Dobrynin–Konkolewicz model are marked with blue dots (strain rate = 0.0067 1/s) and red dash lines (strain rate = 0.106 1/s).

the modulus pre-factors. The fits are included in Figure 6 and we refer to the Supplementary data file Section 6 for further details. For the DN, the long time scale in the Maxwell model is replaced by a constant that represents the contribution of the permanent cross-links to the modulus.

To extrapolate the activation energy from the hydrogen bond relaxation time, the Arrhenius equation is applied as follows:

TABLE 5 Activation energy according to different extrapolation methods.

E_a (kJ/mol)	Transient network	Dual network	Reference
Rheology shift factor	111	—	79
Dielectric	74	—	47
Maxwell model	92	120	—

TABLE 6 Hydrogen bond relaxation time at T = −25 ° C from different extrapolation methods.

τ (s)	TN	DN
Dielectric (τ_{α^*})	2.11	11.5
Maxwell model (τ_{mx})	1.41	3.98
Dobrynin–Konkolewicz (τ_{DK})	—	3.66–24.56

$$\tau_t \approx \tau_{0,m} \exp\left(\frac{E_a}{k_b T}\right), \tag{18}$$

where E_a is the activation energy, k_b is the Boltzmann constant, T is the temperature, and $\tau_{0,m}$ is the minimum attempt time. Figure 7 shows the relaxation time of hydrogen bonds plotted with the inverse of temperature. The activation energy obtained from the Maxwell model fitting yields an activation energy of 92 kJ/mol for the TN and 120 kJ/mol for the DN. It is important to note that the activation energy is not only affected by the energy of association for hydrogen bonds but also by the time required for a molecule to switch partners. This effect becomes less pronounced at higher temperatures, as the energy potential well becomes lesser. At high temperatures, the hydrogen bonds are inactive, so the relaxation times of the hydrogen bond in both cases are close to identical. Thus, the difference of 28 kJ/mol is the increased potential energy arising from the contribution of permanent crosslinking. The results show that dual networks could obtain a different temperature response by applying static linkers. Permanent crosslinks not only could preserve the topology of a network but also enhance the strength of transient crosslinks, allowing higher strains at the break.

3.4 Small deformation stretch

The relationship between the Thy–DAT bond lifetime, activation energy, and modulus in a quiescent state has been discussed at length in the previous sections. To discuss the characteristics of transient bonds in energy dissipation (Hu et al, 2017) and the relationship of bond lifetime in anisotropic stretching, the recent Dobrynin–Konkolewicz model (Carrillo et al, 2013; Bennett et al, 2022) is applied. The microscale bond lifetime and the macroscale rubber mechanical properties of the DN in the small deformation range of a stress–strain experiment with varying strain rates lead to

$$\sigma(\lambda,\dot{\lambda}) = \frac{G(\lambda,\dot{\lambda})}{3}\left[\lambda - \frac{1}{\lambda^2}\right]\left[1 + 2\left(1 - \frac{\beta I_1(\lambda)}{3}\right)\right]^{-2} + \frac{\partial G(\lambda,\dot{\lambda})}{\partial \lambda}\left[\frac{I_1(\lambda)}{6} + \frac{1}{\beta}\left(1 - \frac{\beta I_1(\lambda)}{3}\right)^{-1} - C\right], \tag{19}$$

$$\frac{\partial G(\lambda,\dot{\lambda})}{\partial \lambda} = -\frac{-G_t}{\dot{\lambda}\tau}\left(\frac{\lambda - 1}{\dot{\lambda}\tau} + 1\right)^{-2}, \tag{20}$$

$$G(\lambda,\dot{\lambda}) = G_p + G_t\left(\frac{\lambda - 1}{\dot{\lambda}\tau} + 1\right)^{-1}. \tag{21}$$

The model assumes that transient bonds within a covalent network will cause the total crosslink density to diminish during uniaxial stretching. The lifetime or relaxation time of the TN, denoted as τ_{DK}, depends solely on the rate of deformation during stretching. G_t and G_p represent the shear modulus contributions from both transient and permanently crosslinked networks, respectively. The extension ratio, denoted as λ, i.e., L/L0 is defined as a function of the strain rate, $\lambda = 1 + \dot{\varepsilon}t$. t is the time and the strain rate of stretching the network is denoted as $\dot{\lambda} = \dot{\varepsilon}$. The first strain invariant for uniaxial elongation, denoted as $I_1(\lambda)$, is expressed as $I_1(\lambda) = \lambda^2 + 2\lambda^{-1}$. C is a normalization constant and is given as follows:

$$C = \frac{1}{2} + \frac{1}{\beta(1-\beta)} \tag{22}$$

where β represents the strain hardening parameter, which is the ratio of the mean-squared end-to-end length. Since the system is only investigated under small deformations, the β value is fixed to the computed value of 0.005 for our system to account for the low sensitivity of fitting to the small deformation range. The overall fitting curve and table are shown in Figure 8; Table 4. We assume that the contribution of the entanglement modulus, G_e, is of minor importance in this case, an assumption at least valid for the highest strain rates. We neglect this part and treat the contribution only as a fraction of G_p.

The fitting results show a good agreement with the permanent G_p value, and the crosslink density corresponds well to the calculated crosslink density from the network swelling (Table 1), yielding a mesh size of 20,200 g/mol.

Figures 9A, B present the strain rate relationship with G_t and G_p and the strain rate relationship with G_{tot}, which is the sum of G_t and G_p. The increase in the transient G_t depends naturally on the deformation rate. When the stretching speed is fast and exceeds the inverse bond lifetime, i.e., $\dot{\varepsilon}\tau \geq 1$, the transient bonds stretch along as they have not yet undergone scission, resulting in a higher total modulus of the material due to the unrelaxed TN part. In contrast, for low stretching rates, i.e., $\dot{\varepsilon}\tau \leq 1$, the modulus is lowered due to the cleavage of transient bonds. Considering the former lifetimes of around 1 s at −25°C for the TN or using 3 s for the DN, a rate of 1.0 to 0.3/s would be at least needed. The fitted value of G_{tot} and of τ_{DK} agree extremely well with the DMA results (Supplementary Figure S20). The lifetime of the temporary crosslinks, denoted by τ_{DK}, and from the peak position of the

loss modulus in both DMA and rheology curves, is consistent and enclose the dissipation peak of the H-bond opening (Figure 9C). Neglecting the entanglement modulus does not interfere with the bond lifetime extraction and corroborates the interpretation (Jacobs et al, 2021). We boldly conclude that the strain for a Thy–DAT complex to break is therefore of the order of 10%, which is visually the deformation at which the initial affine deformation modulus bends down. The ratio of lifetimes $\tau_{DK,T=-35℃}/\tau_{DK,T=-25℃}$ is smaller than the shift factor, however obtained in linear rheology or DMA, which can be attributed to the non-equilibrium state of the system where strain is applied in an uniaxial direction.

4 Conclusion and outlook

In the former, we have explored the evolution of dynamic properties in the transition from inactive polymer blends to supramolecular-active TNs, and finally to dual networks that combine all aspects simultaneously. The value of such a system over conventional elastomers lies in a novel responsiveness to both strain and time. The introduction of permanent crosslinks to an H-bonded chain mixture, where the different topologies that are present in the bulk are preserved and quenched, induces a clear shift toward considerably longer bonding times of the Thy–DAT complex. We refer to a summary of parameters in Tables 5, 6. The activation energy of dissociation of the Thy–DAT stickers and the lifetime of the closed state are consistently higher as the stickers have a higher probability to remain at the same partner. All independent methods in this study are in agreement with this unexpected result. Apparently, the increased confinement or at least the stronger restriction of the configuration space within the elastic meshes is responsible for the longer stability of the triple H-bond that is formed in the Thy–DAT association. Despite the individually different sensitivities of the methods to the original aim of the investigation, i.e., to produce an idealized model-dual dynamic network, conclusions can be safely drawn: supramolecular hydrogen bonds can be introduced as sacrificial but repeatable units to control the modulus of the rubber between soft and strong. For frequencies of the order of 1 Hz, or strain rates of the order of 1.0/s, the critical strain-at-rupture of the triple H-bonds is identified to be about 10% in our example. Although the hetero-association of both nucleobase-like groups certainly depends on the immediate environment (matching polarity, competing interactions, solvents. . .), this strain should be a parameter that is grossly independent of the environment and could be verified from *ab initio* methods or molecular dynamics simulations.

Furthermore, whereas the timely response of the DN is already of interest, e.g., shock damping materials or common tire specifications, this level of strain—under static or dynamic excitation—is also important. We have already discussed in the introduction how most common daily life elastomers can benefit from our study. The tire tread rubber is highly filled, and many reinforcing mechanisms are involved to arrive at the final properties. These typical properties are, however, counter-acting and if some are optimized, the others are influenced negatively. The well-known Payne effect in filled rubbers, which is due to the breaking-and-reforming of filler aggregates, is connected with a reduction of the storage modulus and loss of elastic behavior which becomes clear through a pronounced dissipation peak. The engine will consume more fuel as the resistance with the road is increased. The strain range, at which the loss modulus peaks in the thread, coincides with the estimated breaking strain from the static stress–strain model. In addition, the microscopic times applied to a tire running at an average speed of 100 km/h and typical loading degrees of the filler of about 100 phr are well-caught. The confinement that these fillers induce seems to be of the same order of magnitude as the spacing in our model system, i.e., elastic chain lengths of the order of 1,000–4,000 g/mol corresponding to ~2–8 nm. Thus, considerable improvements could be obtained in the future. The aforementioned example does not involve any further time-dependent mechanisms. Modifying the thread component with supramolecular functions comparable to the Thy–DAT combination would be able to compensate for the (low frequency) Payne effect by adding the transient modulus to the chemical crosslinking modulus without destroying the high-frequency properties like wet skid that come into play at large deformations where the H-bonds have sacrificed already. Since the modulus, however, decreases with temperature, an increase of the elastic modulus due to the H-bonding interactions could have a decisive positive effect on the overall performance of such a dual-rubber-based tire. In the future, H-bonding groups like ours can be grafted onto a typical silica filler surface and dispersed into a non- or supramolecular-modified elastomer. The direct consequence of all these is the reduction of hysteresis at small strains, restoring elasticity while minimizing cracks and its development at large deformations. Key processes may be developed to adjust the desired mechanical properties for useful materials in day-to-day life. A forthcoming study will focus on the structure and its change upon uniaxial deformation using *in situ* small angle X-ray and neutron scattering.

Data availability statement

The original contributions presented in the study are included in the article/Supplementary Material. Further inquiries can be directed to the corresponding authors.

Author contributions

Conceptualization, WP-H; data acquisition, JF, JA, and MK; discussion, JF, JA, MK, SF, and WP-H; formal analysis, JF; investigation, JF and WP-H; visualization, JF; writing the original draft, JF; writing—review and editing, JF, JA, and WP-H; supervision, SF and WP-H; funding acquisition, SF and WP-H; project administration, SF and WP-H. All authors contributed to the article and approved the submitted version.

Acknowledgments

JF expresses gratitude to Dr. Aakash Sharma and Dr. Tulika Sharma for their valuable contributions in the form of insightful discussions and meticulous proofreading. Dr. Andreas Raba is thanked for the synthesis of the DAT-F component.

Conflict of interest

The authors declare that the research was conducted in the absence of any commercial or financial relationships that could be construed as a potential conflict of interest.

Publisher's note

All claims expressed in this article are solely those of the authors and do not necessarily represent those of their affiliated organizations, or those of the publisher, the editors, and the reviewers. Any product that may be evaluated in this article, or claim that may be made by its manufacturer, is not guaranteed or endorsed by the publisher.

Supplementary material

The Supplementary Material for this article can be found online at: https://www.frontiersin.org/articles/10.3389/frsfm.2023.1221803/full#supplementary-material

References

Ahmadi, M., Jangizehi, A., Saalwächter, K., and Seiffert, S. (2023). Effect of Junction aggregation on the dynamics of supramolecular polymers and networks. *Macromol. Chem. Phys.* 224, 2200389. doi:10.1002/macp.202200389

Ahmadi, M., Jangizehi, A., and Seiffert, S. (2022). Backbone polarity tunes sticker clustering in hydrogen-bonded supramolecular polymer networks. *Macromolecules* 55, 5514–5526. doi:10.1021/acs.macromol.2c00645

Allgaier, J., Hövelmann, C. H., Wei, Z., Staropoli, M., Pyckhout-Hintzen, W., Lühmann, N., et al. (2016). Synthesis and rheological behavior of poly(1,2-butylene oxide) based supramolecular architectures. *R. Soc. Chem.* 6, 6093–6106. doi:10.1039/c5ra24547h

Awaja, F., Zhang, S., Tripathi, M., Nikiforov, A., and Pugno, N. (2016). Cracks, microcracks and fracture in polymer structures: Formation, detection, autonomic repair. *Prog. Mater. Sci.* 83, 536–573. doi:10.1016/j.pmatsci.2016.07.007

Barrera, C. S., and Tardiff, J. L. (2022). Static and dynamic properties of eggshell filled natural rubber composites for potential application in automotive vibration isolation and damping. *J. Clean. Prod.* 353, 131656. doi:10.1016/j.jclepro.2022.131656

Bennett, C., Hayes, P. J., Thrasher, C. J., Chakma, P., Wanasinghe, S. V., Zhang, B., et al. (2022). Modeling approach to capture hyperelasticity and temporary bonds in soft polymer networks. *Macromolecules* 55, 3573–3587. doi:10.1021/acs.macromol.1c02319

Bentz, K. C., and Cohen, S. M. (2018). Supramolecular metallopolymers: From linear materials to infinite networks. *Angew. Chem. Int. Ed.* 57, 14992–15001. doi:10.1002/anie.201806912

Brás, A. R., Hövelmann, C. H., Antonius, W., Teixeira, J., Radulescu, A., Allgaier, J., et al. (2013). Molecular approach to supramolecular polymer assembly by small angle neutron scattering. *Macromolecules* 46, 9446–9454. doi:10.1021/ma401714r

Carrillo, J. M. Y., Mackintosh, F. C., and Dobrynin, A. V. (2013). Nonlinear elasticity: From single chain to networks and gels. *Macromolecules* 46, 3679–3692. doi:10.1021/ma400478f

Chandra, A. K., and Kumar, N. R. (2017). "Polymer nanocomposites for automobile engineering applications," in *Properties and applications of polymer nanocomposites: Clay and carbon based polymer nanocomposites*. Editors D. K. Tripathy and B. P. Sahoo (Berlin, Heidelberg: Springer Berlin Heidelberg), 139–172.

Chen, Q., Zhang, Z., and Colby, R. H. (2016). Viscoelasticity of entangled random polystyrene ionomers. *J. Rheology* 60, 1031–1040. doi:10.1122/1.4955432

Cortese, J., Soulie-Ziakovic, C., Cloitre, M., Tencé-Girault, S., and Leibler, L. (2011). Order-disorder transition in supramolecular polymers. *J. Am. Chem. Soc.* 133, 19672–19675. doi:10.1021/ja209126a

Cortese, J., Soulie-Ziakovic, C., Tencé-Girault, S., and Leibler, L. (2012). Suppression of mesoscopic order by complementary interactions in supramolecular polymers. *J. Am. Chem. Soc.* 134, 3671–3674. doi:10.1021/ja2119496

Doi, M., and Edwards, S. (1978). Dynamics of concentrated polymer systems. Part 1.—brownian motion in the equilibrium state. *J. Chem. Soc. Faraday Trans. 2 Mol. Chem. Phys.* 74, 1789–1801. doi:10.1039/f29787401789

Friedrich, K., and Almajid, A. A. (2013). Manufacturing aspects of advanced polymer composites for automotive applications. *Appl. Compos. Mater.* 20, 107–128. doi:10.1007/s10443-012-9258-7

Gałązka, M., and Osiecka-Drewniak, N. (2022). Electric conductivity and electrode polarization as markers of phase transitions. *Crystals* 12, 1797. doi:10.3390/cryst12121797

Ge, S., Tress, M., Xing, K., Cao, P.-F., Saito, T., and Sokolov, A. P. (2020). Viscoelasticity in associating oligomers and polymers: Experimental test of the bond lifetime renormalization model. *Soft Matter* 16, 390–401. doi:10.1039/c9sm01930h

Gerstl, C., Schneider, G. J., Pyckhout-Hintzen, W., Allgaier, J., Richter, D., Alegría, A., et al. (2010). Segmental and normal mode relaxation of poly(alkylene oxide)s studied by dielectric spectroscopy and rheology. *Macromolecules* 43, 4968–4977. doi:10.1021/ma100384j

Glomann, T., Schneider, G. J., Brás, A. R., Pyckhout-Hintzen, W., Wischnewski, A., Zorn, R., et al. (2011). Unified description of the viscoelastic and dielectric global chain motion in terms of the tube theory. *Macromolecules* 44, 7430–7437. doi:10.1021/ma200674z

Gold, B. J., Hövelmann, C. H., Weiss, C., Radulescu, A., Allgaier, J., Pyckhout-Hintzen, W., et al. (2016). Sacrificial bonds enhance toughness of dual polybutadiene networks. *Polymer* 87, 123–128. doi:10.1016/j.polymer.2016.01.077

Goldansaz, H., Fustin, C.-A., Wübbenhorst, M., and Van Ruymbeke, E. (2016). How supramolecular assemblies control dynamics of associative polymers: Toward a general picture. *Macromolecules* 49, 1890–1902. doi:10.1021/acs.macromol.5b01535

Hamed, G. R. (2000). Reinforcement of rubber. *Rubber Chem. Technol.* 73, 524–533. doi:10.5254/1.3547603

Havriliak, S., and Negami, S. (1967). A complex plane representation of dielectric and mechanical relaxation processes in some polymers. *Polymer* 8, 161–210. doi:10.1016/0032-3861(67)90021-3

Herbst, F., Schröter, K., Gunkel, I., Gröger, S., Thurn-Albrecht, T., Balbach, J., et al. (2010). Aggregation and chain dynamics in supramolecular polymers by dynamic rheology: Cluster formation and self-aggregation. *Macromolecules* 43, 10006–10016. doi:10.1021/ma101962y

Hu, X., Zhou, J., Daniel, W. F. M., Vatankhah-Varnoosfaderani, M., Dobrynin, A. V., and Sheiko, S. S. (2017). Dynamics of dual networks: Strain rate and temperature effects in hydrogels with reversible H-bonds. *Macromolecules* 50, 652–659. doi:10.1021/acs.macromol.6b02422

Jacobs, M., Liang, H., and Dobrynin, A. V. (2021). Theory and simulations of hybrid networks. *Macromolecules* 54, 7337–7346. doi:10.1021/acs.macromol.1c00774

Jiang, Y., Wang, Y. X., Wang, S. Z., and Su, X. W. (2014). "Frequency dependence stiffness and damping of "O" rubber ring," in *Advanced materials research*, 368–372.

Katashima, T. (2021). Rheological studies on polymer networks with static and dynamic crosslinks. *Polym. J.* 53, 1073–1082. doi:10.1038/s41428-021-00505-y

Kawano, S., Nakano, K., Sato, H., Muraoka, M., and Shizuma, M. (2022). Photo- and thermo-responsive supramolecular polymer networks via *in situ* polymerization using homoternary macrocyclic host with coumarin monomers in water. *Polym. Chem.* 13, 5820–5828. doi:10.1039/d2py00952h

Krutyeva, M., Brás, A. R., Antonius, W., Hövelmann, C. H., Poulos, A. S., Allgaier, J., et al. (2015). Association behavior, diffusion, and viscosity of end-functionalized supramolecular poly(ethylene glycol) in the melt state. *Macromolecules* 48, 8933–8946. doi:10.1021/acs.macromol.5b02060

Lange, R. F. M., Van Gurp, M., and Meijer, E. W. (1999). Hydrogen-bonded supramolecular polymer networks. *J. Polym. Sci. Part A Polym. Chem.* 37, 3657–3670. doi:10.1002/(sici)1099-0518(19991001)37:19<3657::aid-pola1>3.0.co;2-6

Le Bohec, M., Banère, M., Piogé, S., Pascual, S., Benyahia, L., and Fontaine, L. (2016). Sol–gel reversible metallo-supramolecular hydrogels based on a thermoresponsive double hydrophilic block copolymer. *Polym. Chem.* 7, 6834–6842. doi:10.1039/c6py01639a

Lee, M., Moore, R. B., and Gibson, H. W. (2011). Supramolecular pseudorotaxane graft copolymer from a crown ether polyester and a complementary paraquat-terminated polystyrene guest. *Macromolecules* 44, 5987–5993. doi:10.1021/ma201241t

Leibler, L., Rubinstein, J. M., and Colby, R. H. (1991). Dynamics of reversible networks. *Macromolecules* 24, 4701–4707. doi:10.1021/ma00016a034

Li, X., Kuang, Y., Lin, H.-C., Gao, Y., Shi, J., and Xu, B. (2011). Supramolecular nanofibers and hydrogels of nucleopeptides. *Angew. Chem. Int. Ed.* 50, 9365–9369. doi:10.1002/anie.201103641

Mcleish, T. C. B. (2002). Tube theory of entangled polymer dynamics. *Adv. Phys.* 51, 1379–1527. doi:10.1080/00018730210153216

Monkenbusch, M., Krutyeva, M., Pyckhout-Hintzen, W., Antonius, W., Hövelmann, C. H., Allgaier, J., et al. (2016). Molecular view on supramolecular chain and association dynamics. *Phys. Rev. Lett.* 117, 147802. doi:10.1103/physrevlett.117.147802

Mozhdehi, D., Neal, J. A., Grindy, S. C., Cordeau, Y., Ayala, S., Holten-Andersen, N., et al. (2016). Tuning dynamic mechanical response in metallopolymer networks through simultaneous control of structural and temporal properties of the networks. *Macromolecules* 49, 6310–6321. doi:10.1021/acs.macromol.6b01626

Murphy, E. B., and Wudl, F. (2010). The world of smart healable materials. *Prog. Polym. Sci.* 35, 223–251. doi:10.1016/j.progpolymsci.2009.10.006

Nicolella, P., Lauxen, D., Ahmadi, M., and Seiffert, S. (2021). Reversible hydrogels with switchable diffusive permeability. *Macromol. Chem. Phys.* 222, 2100076. doi:10.1002/macp.202100076

Pappalardo, A., Ballistreri, F. P., Destri, G. L., Mineo, P. G., Tomaselli, G. A., Toscano, R. M., et al. (2012). Supramolecular polymer networks based on calix[5]arene tethered poly(p-phenyleneethynylene). *Macromolecules* 45, 7549–7556. doi:10.1021/ma3015239

Riedel, C., Alegría, A., Tordjeman, P., and Colmenero, J. (2010). High and low molecular weight crossovers in the longest relaxation time dependence of linear cis-1,4 polyisoprene by dielectric relaxations. *Rheol. Acta* 49, 507–512. doi:10.1007/s00397-010-0433-1

Saintier, N., Cailletaud, G., and Piques, R. (2011). Cyclic loadings and crystallization of natural rubber: An explanation of fatigue crack propagation reinforcement under a positive loading ratio. *Mater. Sci. Eng. A* 528, 1078–1086. doi:10.1016/j.msea.2010.09.079

Schaefer, C., Laity, P. R., Holland, C., and Mcleish, T. C. B. (2020). Silk protein solution: A natural example of sticky reptation. *Macromolecules* 53, 2669–2676. doi:10.1021/acs.macromol.9b02630

Shahid, T., Huang, Q., Oosterlinck, F., Clasen, C., and Van Ruymbeke, E. (2017). Dynamic dilution exponent in monodisperse entangled polymer solutions. *Soft Matter* 13, 269–282. doi:10.1039/c6sm01083k

Shangguan, Y., Yang, J., and Zheng, Q. (2017). Rheology of nitrile rubber with hybrid crosslinked network composed of covalent bonding and hydrogen bonding. *RSC Adv.* 7, 15978–15985. doi:10.1039/c7ra01106g

Shoda, Y., Aoki, D., Tsunoda, K., and Otsuka, H. (2020). Polybutadiene rubbers with urethane linkages prepared by a dynamic covalent approach for tire applications. *Polymer* 202, 122700. doi:10.1016/j.polymer.2020.122700

Staropoli, M., Kruteva, M., Allgaier, J., Wischnewski, A., and Pyckhout-Hintzen, W. (2020). Supramolecular dimerization in a polymer melt from small-angle X-ray scattering and rheology: A miscible model system. *Polymers* 12, 880. doi:10.3390/polym12040880

Staropoli, M., Raba, A., Hövelmann, C. H., Krutyeva, M., Allgaier, J., Appavou, M.-S., et al. (2016). Hydrogen bonding in a reversible comb polymer architecture: A microscopic and macroscopic investigation. *Macromolecules* 49, 5692–5703. doi:10.1021/acs.macromol.6b00978

Stockmayer, W. H. (1967). Dielectric dispersion in solutions of flexible polymers. *Pure Appl. Chem.* 15, 539–554. doi:10.1351/pac196715030539

Suslick, B. A., Hemmer, J., Groce, B. R., Stawiasz, K. J., Geubelle, P. H., Malucelli, G., et al. (2023). Frontal polymerizations: From chemical perspectives to macroscopic properties and applications. *Chem. Rev.* 123, 3237–3298. doi:10.1021/acs.chemrev.2c00686

Urakawa, O., Yamane, M., Tomie, S., Inoue, T., Shikata, T., and Adachi, K. (2018). Relationship between global and segmental dynamics of poly(butylene oxide) studied by broadband dielectric spectroscopy. *J. Chem. Phys.* 148, 034904. doi:10.1063/1.5006364

Vahdati, N., and Saunders, L. K. L. (2002). High frequency testing of rubber mounts. *ISA Trans.* 41, 145–154. doi:10.1016/s0019-0578(07)60074-3

Van Gemert, G. M. L., Peeters, J. W., Söntjens, S. H. M., Janssen, H. M., and Bosman, A. W. (2011). Self-healing supramolecular polymers in action. *Macromol. Chem. Phys.* 213, 234–242. doi:10.1002/macp.201100559

Van Krevelen, D. W., and Te Nijenhuis, K. (2009). "Chapter 7 - cohesive properties and solubility," in *Properties of polymers*. Editors D. W. Van Krevelen and K. Te Nijenhuis. 4 (Amsterdam: Elsevier), 189–227.

Van Ruymbeke, E., Shchetnikava, V., Matsumiya, Y., and Watanabe, H. (2014). Dynamic dilution effect in binary blends of linear polymers with well-separated molecular weights. *Macromolecules* 47, 7653–7665. doi:10.1021/ma501566w

Vereroudakis, E., Bantawa, M., Lafleur, R. P. M., Parisi, D., Matsumoto, N. M., Peeters, J. W., et al. (2020). Competitive supramolecular associations mediate the viscoelasticity of binary hydrogels. *ACS Central Sci.* 6, 1401–1411. doi:10.1021/acscentsci.0c00279

Verjans, J., André, A., Van Ruymbeke, E., and Hoogenboom, R. (2022). Physically cross-linked polybutadiene by quadruple hydrogen bonding through side-chain incorporation of ureidopyrimidinone with branched alkyl side chains. *Macromolecules* 55, 928–941. doi:10.1021/acs.macromol.1c01908

Vogel, D. H. (1921). Das temperaturabhaengigkeitsgesetz der Viskositaet von Fluessigkeiten. *Phys. Z.* 22, 645. doi:10.4236/ojn.2014.43019

Watanabe, H. (2001). Dielectric relaxation of type-A polymers in melts and solutions. *Macromol. Rapid Commun.* 22, 127–175. doi:10.1002/1521-3927(200102)22:3<127::aid-marc127>3.0.co;2-s

Wu, S., and Chen, Q. (2022). Advances and new opportunities in the rheology of physically and chemically reversible polymers. *Macromolecules* 55, 697–714. doi:10.1021/acs.macromol.1c01605

Wübbenhorst, M., and Van Turnhout, J. (2002). Analysis of complex dielectric spectra. I. One-dimensional derivative techniques and three-dimensional modelling. *J. Non-Crystalline Solids* 305, 40–49. doi:10.1016/s0022-3093(02)01086-4

Xie, Z., Hu, B.-L., Li, R.-W., and Zhang, Q. (2021). Hydrogen bonding in self-healing elastomers. *ACS Omega* 6, 9319–9333. doi:10.1021/acsomega.1c00462

Yamane, M., Hirose, Y., and Adachi, K. (2005). Dielectric normal and segmental modes in undiluted poly(butylene oxide). *Macromolecules* 38, 9210–9215. doi:10.1021/ma0516384

Zhang, Z., Huang, C., Weiss, R. A., and Chen, Q. (2017). Association energy in strongly associative polymers. *J. Rheology* 61, 1199–1207. doi:10.1122/1.4997586